Analysis of Sub-Grid Modelling for LES of Supercritical Flows

By E. S. Richardson†, M. Jarczyk‡, S. Pohl‡ AND M. Pfitzner‡

†Faculty of Engineering and the Environment, University of Southampton, United Kingdom
‡Institute for Thermodynamics, Universität der Bundeswehr München, Germany

The thermodynamic and transport properties of fluids above their critical pressure deviate significantly from those of an ideal gas. This numerical study addresses the effect of real gas properties on the behaviour and Large Eddy Simulation (LES) modelling of supercritical flow. The focus is on thermal mixing in nitrogen, above the critical pressure, but spanning the pseudo-boiling temperature; modelling of these conditions is challenging because they exhibit steep gradients of density and other physical properties. Applying a volume-corrected Peng-Robinson real-gas equation of state and real-gas transport models, three supercritical flow configurations have been considered. The simplest involves a thermally inhomogeneous constant pressure system; the second, thermal mixing in a laminar counterflow; and third, a LES of a turbulent jet of cold nitrogen mixing with a hot environment. The analysis leads to two novel conclusions for transcritical flows. First, it has been shown that at low temperatures close to the pseudo-boiling temperature, the LES filtered density depends strongly on sub-filter temperature variance, and consequently that thermal dissipation leads to a source term for filtered density. Second, that sub-filter temperature stratification causes anisotropy in the effective molecular viscosity – reducing the effective viscosity for shear normal to the temperature gradient, and similarly reducing the effective thermal conductivity below its mean value. It is found, however, that the LES methodology presented here predicts the mean density profile of the turbulent nitrogen jet adequately, even though the LES modelling neglects sub-grid property fluctuations.

1. Introduction

Supercritical fluid injection occurs in combustion systems operating at high pressures; examples include rocket engine combustors and high compression ratio jet engines at take-off conditions. Further understanding of supercritical fluid injection is desired in order to improve predictive models for engine performance. Fluid behaviour at high pressure deviates from that of a perfect gas, and this leads to differences in the way turbulent mixing occurs and to how it should be modelled [1–4]. In the context of Large Eddy Simulation (LES) of turbulent mixing, sub-grid closures are required to describe the effects of unresolved mixing processes. The objective of the collaborative study described in this report is to investigate how the properties of supercritical fluid influence small-scale mixing, and to consider their impact on sub-grid modelling for LES.

Analysis of direct numerical simulation (DNS) results indicates that modelling of turbulent supercritical fluids becomes significantly more challenging when compositional or thermal inhomogeneity lead to large property gradients within the flow [2, 4], compared to flows without large compositional or thermal variations [3]. In order to isolate

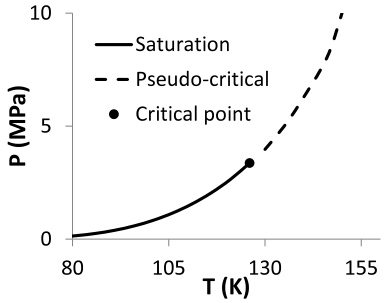

FIGURE 1. Phase diagram of nitrogen showing the saturation curve, critical point, and the pseudo-boiling line. Data from NIST [6].

the effects of steep property gradients and to accentuate the associated modelling challenges, this study focuses on thermal mixing in a single-component fluid at transcritical conditions. In particular we follow the experimental work by Mayer *et al.* [5] and consider nitrogen at a supercritical pressure of 3.97 MPa. This experimental configuration, which has been modelled using LES in this study, contains a temperature range (127 to 298 K) which spans the pseudo-boiling temperature (130 K at 3.97 MPa). The pseudo-boiling temperature occurs at the maximum value of heat capacity, at a given pressure. On the nitrogen temperature-pressure phase diagram in Fig. 1, the locus of pseudo-boiling temperature is a continuation of the liquid-gas equilibrium line into the supercritical region.

These thermodynamic conditions (referred to as *transcritical* on account of spanning the pseudo-boiling temperature) give a density variation from 433 to 45 kg/m^3. The thermal conductivity and the constant pressure heat capacity also vary by an order of magnitude [6]. The supercritical experiments by Mayer and coworkers have been the target of numerous numerical simulations. The experimental configuration has been computed by LES (for example in the work of Ribert *et al.* in the current proceedings [7]), and the thermodynamic conditions from the experiments have also been studied using Direct Numerical Simulation [2].

This report proceeds in Sec. 2 with an introduction to the effects of supercritical fluid properties on mixing and the associated closures that are required for LES of supercritical flow. In Sec. 3 the numerical simulation methods used in this study are presented and, in Sec. 4 the simulation results are analysed in order to investigate sub-grid closure for LES.

2. Modelling for supercritical LES

Large Eddy Simulation involves solution of spatially filtered conservation equations, requiring closure models to account for the influence of unresolved – sub-filter-scale or sub-grid-scale (SGS) – processes.

2.1. *Conservation equations*

The general conservation equations for a compressible pure component flow are:

$$\frac{\partial \rho}{\partial t} + \frac{\partial \rho u_j}{\partial x_j} = 0, \tag{2.1}$$

$$\frac{\partial \rho u_i}{\partial t} + \frac{\partial \rho u_i u_j}{\partial x_j} = -\frac{\partial p}{\partial x_i} + \frac{\partial \sigma_{ij}}{\partial x_j} \ , \tag{2.2}$$

and expressing energy conservation in terms of the specific enthalpy h:

$$\frac{\partial \rho h}{\partial t} + \frac{\partial \rho u_j h}{\partial x_j} = -\frac{\partial q_j}{\partial x_j} + \frac{\partial \sigma_{ij} u_i}{\partial x_j} + \frac{Dp}{Dt}. \tag{2.3}$$

Here x_j are Cartesian coordinates, t is the time, ρ is the density, u_i is the velocity component in direction i, and p is the thermodynamic pressure. q_j is the heat flux vector and σ_{ij} represents the viscous stress tensor. Einstein summation is applied to repeated Roman subscripts. The heat flux is modeled by Fick's law with

$$q_j = -\lambda \frac{\partial T}{\partial x_j}. \tag{2.4}$$

Here λ is the thermal conductivity. The viscous stress tensor for a Newtonian fluid is defined by

$$\sigma_{ij} = 2\mu \left(S_{ij} - \frac{1}{3} S_{kk} \delta_{ij} \right), \tag{2.5}$$

where μ is the dynamic viscosity and the strain-rate tensor S_{ij} is

$$S_{ij} = \frac{1}{2} \left(\frac{\partial u_i}{\partial x_j} + \frac{\partial u_j}{\partial x_i} \right). \tag{2.6}$$

Assuming thermodynamic equilibrium the thermodynamic variables (h, p, T, and ρ) can be expressed as a function of any other two independent thermodynamic variables in the local state vector ϕ using a characteristic equation of state. The transport coefficients, μ and λ, appearing in molecular flux terms are also a function of the local thermodynamic state ϕ.

2.2. *LES modelling*

The LES differential equations are obtained by filtering Eqs. (2.1)-(2.3) under the assumption that filtering and differentiation commute:

$$\frac{\partial \bar{\rho}}{\partial t} + \frac{\partial \bar{\rho} \tilde{u}_j}{\partial x_j} = 0, \tag{2.7}$$

$$\frac{(\bar{\rho} \tilde{u}_i)}{\partial t} + \frac{\partial \left(\overline{\rho u_i u_j} \right)}{\partial x_j} = -\frac{\partial \bar{p}}{\partial x_i} + \frac{\partial \bar{\sigma}_{ij}}{\partial x_j} - \frac{\partial \bar{\rho} \tau_{ij}}{\partial x_j}, \tag{2.8}$$

$$\frac{\partial \bar{\rho} \tilde{h}}{\partial t} + \frac{\partial \overline{\rho u_j h}}{\partial x_j} = -\frac{\partial \bar{q}_j}{\partial x_j} - \frac{\partial \bar{\rho} \zeta_j}{\partial x_j} + \frac{\partial \overline{\sigma_{ij} u_i}}{\partial x_j} - \frac{\partial \bar{\rho} \tau_{ij} \tilde{u}_i}{\partial x_j} + \overline{\frac{Dp}{Dt}}. \tag{2.9}$$

Here $\tilde{(.)}$ represents the density weighted (Favre) filtering operation, and $\bar{(.)}$ represents the unweighted filtering operation.

The SGS fluxes, molecular fluxes, and terms involving the filtered thermodynamic state variables in Eqs. (2.8) and (2.9) are unclosed and require modelling.

2.2.1. *Modelling of sub-grid fluxes*

The sub-grid momentum and enthalpy fluxes respectively are equal to:

$$\tau_{ij} = \widetilde{u_i u_j} - \tilde{u}_i \tilde{u}_j, \tag{2.10}$$

and

$$\zeta_j = \widetilde{u_j h} - \tilde{u_j}\tilde{h}. \tag{2.11}$$

The sub-grid flux terms arise due to unresolved velocity fluctuations, and it is their closure that usually receives the most attention in incompressible or ideal-gas flows, for example [8–10]. For supercritical flow, Taskinoglu *et al.* [4] have evaluated the performance of various SGS flux models which were previously validated in ideal-gas or incompressible flows. Further evaluation and validation of the available SGS flux models is still required for turbulent flow across a wide range of supercritical conditions. The progress of SGS flux model validation for supercritical flows is restricted partly by the limited availability of high-fidelity numerical or experimental data for validation purposes, and turbulent SGS flux modelling is not addressed directly in this study.

2.2.2. *Evaluation of filtered thermodynamic properties*

The influence of the unclosed terms other than the SGS fluxes is usually considered secondary, and the influence of sub-grid variations of thermodynamic and transport properties are commonly neglected, leading to the assumption that these properties are a function of the filtered state variable vector:

$$h = h(\bar{\phi}), p = p(\bar{\phi}), T = T(\bar{\phi}), \rho = \rho(\bar{\phi}), \mu = \mu(\bar{\phi}), \lambda = \lambda(\bar{\phi}). \tag{2.12}$$

In supercritical flows, however, the contribution of sub-grid property variations may be significant for LES modelling.

Selle *et al.* [1] provide an *a priori* analysis of the filtered pressure gradient term in Eq. (2.8), finding that the standard closure $p = p(\bar{\phi})$ is inaccurate. Selle *et al.* [1] and then Taskinoglu *et al.* [4] have suggested improved models for the evaluation of the filtered pressure. The 'first-order' model by Taskinoglu *et al.* [4] results from a first-order Taylor expansion:

$$\overline{p(\phi)} \approx \overline{p(\bar{\phi})} + \left.\frac{\partial p}{\partial \phi_m}\right|_{\phi=\bar{\phi}} \left(\overline{\phi_m} - \overline{\overline{\phi_m}}\right). \tag{2.13}$$

Taskinoglu *et al.* [4] find that the first order correction out-performs Selle's model given a LES grid size eight times their DNS grid size. This Taylor expansion modelling can be applied to the evaluation of other filtered thermodynamic and transport properties. Pressure-based solution methods, in contrast to the density-based approach used by Taskinoglu *et al.* , require computation of the filtered density. The corresponding first order density closure,

$$\overline{\rho(\phi)} \approx \overline{\rho(\bar{\phi})} + \left.\frac{\partial \rho}{\partial \phi_m}\right|_{\phi=\bar{\phi}} \left(\overline{\phi_m} - \overline{\overline{\phi_m}}\right), \tag{2.14}$$

has been evaluated below.

2.2.3. *The presumed probability density-function approach*

The statistical variation of sub-grid properties in a supercritical flow can be described using a probability density function (PDF). The presumed-PDF approach is applied frequently to turbulent combustion in order to evaluate filtered quantities (such as the chemical reaction rate) which have a non-linear dependence on sub-filter fluctuations – flamelet modelling [11] being one of its applications. Indeed, flamelet modelling has been applied to combusting supercritical flows [12, 13]. Even without combustion, supercritical fluid properties have strongly non-linear interdependencies (see Fig. 2) and

the presumed-PDF approach may again be useful. The modelling complexity of the presumed-PDF approach increases rapidly with the number of state-space dimensions that are needed in order to accurately describe the sub-grid variation of the flow. Conversely, the presumed-PDF approach is especially useful in two-stream mixing problems (such as the thermal mixing problems studied here) where variations of thermodynamic and transport property variation can be mapped effectively to the variation of a single conserved scalar, so that only the PDF of the conserved scalar needs to be presumed. In the transcritical nitrogen jet of Mayer *et al.* [5] the enthalpy is a conserved scalar and, since the pressure fluctuations in this flow are relatively small, the other properties vary predominantly due to changes in enthalpy. Therefore an alternative to Eq. (2.12) or Eq. (2.14) is to integrate over the probability density function of enthalpy:

$$\overline{\rho(\phi)} \approx \int_{h_0}^{h_1} P(h)\rho(h).dh. \tag{2.15}$$

$P(h)$ is a β-function presumed-PDF [13], defined for the range of enthalpy between the values in the two streams h_0 and h_1. The functional dependence of the fluid properties on the reference variable (h in this case) is obtained from a laminar counterflow simulation between the two streams.

2.2.4. *Evaluation of molecular fluxes*

In well resolved LES the molecular fluxes can have similar magnitude to the sub-grid fluxes and accurate modelling is required. The filtered heat and momentum fluxes, $\bar{q_j}$ and $\bar{\sigma_{ij}}$, are unclosed even if the unclosed filtered transport coefficients $\overline{\lambda(\phi)}$ and $\overline{\mu(\phi)}$ were known. An effective thermal conductivity representing molecular transport at the scale of the LES grid is defined as:

$$\lambda_{\mathrm{mol,j}} = \frac{\overline{q_j}}{\partial\overline{T}/\partial x_j}, \tag{2.16}$$

and the effective dynamic viscosity due to grid-scale molecular transport:

$$\mu_{\mathrm{mol,ij}} = \frac{\overline{\sigma_{ij}}}{\partial\overline{u_i}/\partial x_j}. \tag{2.17}$$

Note that, in general, $\lambda_{\mathrm{mol,j}} \neq \overline{\lambda(\phi)}$ and $\mu_{\mathrm{mol,ij}} \neq \overline{\mu(\phi)}$. It is also notable that the effective transport coefficients depend on direction.

3. Simulation methods

The numerical simulations discussed in this study employ fully consistent real gas models. The study uses two fluid dynamics solvers, both with the same thermodynamic and transport models described below. The thermodynamic and transport models have been implemented by Pohl *et al.* [13] into the COSILAB [14] one-dimensional solver used to study the counterflow configuration. Jarczyk [15] has developed a pressure-based solution method for real-gases within OpenFOAM and this is used for the turbulent jet configuration.

3.1. *Thermodynamic and transport properties*

All thermodynamic properties are calculated as the sum of an ideal reference value and a departure function accounting for real-gas effects based on a real-gas equation of

state. For closure of the system of conservation equations, enthalpy h and constant-pressure specific heat c_p have to be provided. These are defined as

$$h(T,p) = h_0(T) + \int_{p_0}^{p} \left(V - T \left(\frac{\partial V}{\partial T}_p \right) \right) dp, \tag{3.1}$$

and

$$c_p(T,p) = c_v(T,p) - \frac{T \left(\frac{\partial p}{\partial T} \right)_V^2}{\left(\frac{\partial p}{\partial V} \right)_T}. \tag{3.2}$$

The subscript 0 refers to the ideal reference state at low pressure. The departure functions on the right hand side have to be determined using an appropriate equation of state. In the work presented here the Peng-Robinson (PR) equation has been applied [16].

$$p = \frac{RT}{V} - \frac{a(T)}{V^2 + 2bV - b^2}. \tag{3.3}$$

V is the molar volume and R is the universal gas constant with a value of

$$R = 8.314472 J/(mol * K).$$

The constants $a(T)$ and b are calculated from empirical relations. $a(T)$ accounts for attractive forces between the molecules in the fluid and is determined from the empirical equation:

$$a(T) = 0.457235 \frac{R^2 T_c^2}{p_c} . \left(1 - \kappa \left(1 - \sqrt{\frac{T}{T_c}} \right) \right)^2 . \tag{3.4}$$

$\kappa = 0.37464 + 1.54226\omega - 0.26992\omega^2$ is a function of the acentric factor ω. The coefficient

$$b = 0.077796 R T_c / p_c$$

takes into account the effects of the reduction of free volume due to the volume occupied by the molecules. T_c and p_c are the critical temperature and pressure of the modelled species ($N_2 : T_c = 126.192K; p_c = 33.96bar; \omega = 0.0372$). Because the Peng-Robinson equation of state is known to provide poor accuracy in transcritical fluid, an empirical correction method established by Harstad *et al.* [17] has been implemented.

Thermal conductivity and dynamic viscosity have been modeled using empirical correlations for dense fluids developed by Chung *et al.* [18].

The density, specific heat capacity, thermal conductivity and dynamic viscosity models at 3.97 MPa are compared to measured values [6] across the transcritical temperature range in Fig. 2, showing good agreement.

3.2. *Counterflow simulations*

The thermal mixing between two streams of high pressure nitrogen has been studied in an axi-symmetric laminar counterflow. One-dimensional simulations along the centreline of the flow have been performed in physical space using the COSILAB software [14]. The one-dimensional formulation in the axial (y) direction assumes a constant strain rate a_∞ throughout the domain:

$$\frac{\partial \rho}{\partial t} = -\frac{\partial (\rho v)}{\partial y} - 2\rho G \tag{3.5}$$

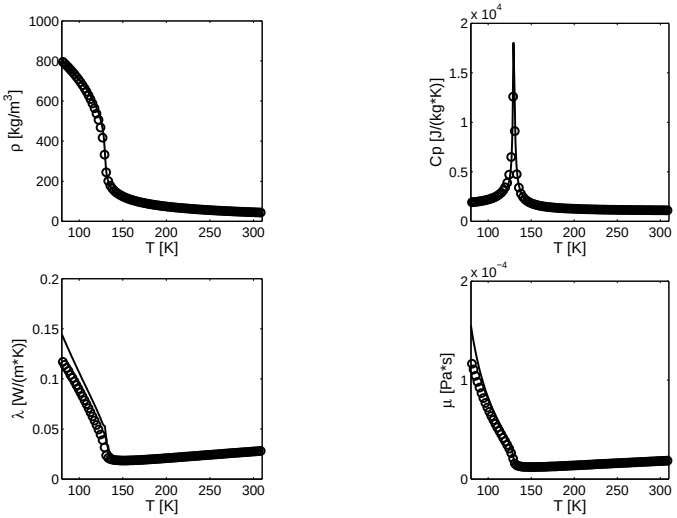

FIGURE 2. Temperature variation of nitrogen's density, heat capacity, thermal conductivity and dynamic viscosity at 3.97 MPa. Data from NIST [6] (symbols) and real gas models from Sec. 3.1 (lines).

$$\rho\frac{\partial G}{\partial t} = \frac{\partial}{\partial y}\left(\mu\frac{\partial G}{\partial y}\right) - \rho v\frac{\partial G}{\partial y} - \rho G^2 + \rho_\infty a_s^2 \tag{3.6}$$

$$\rho\frac{\partial h}{\partial t} = \frac{\partial q_y}{\partial y} - \rho v\frac{\partial h}{\partial y} \tag{3.7}$$

The velocity in the radial (x) direction is denoted u, and the quantity G is defined by u/x.

The solution domain is 0.35mm long. A constant strain rate of 1000s^{-1} and boundary temperatures of 127K and 298K have been applied in order to achieve a steady solution. A mixture fraction is defined for use in the analysis of the counterflow simulation results: the mixture fraction is proportional to enthalpy and it equals zero in the cold stream and unity in the hot stream.

3.3. *LES of transcritical nitrogen injection*

The turbulent nitrogen jet studied by Mayer *et al.* [5] involves a $4.9\,ms^{-1}$ $127K$ (case 3), or a $5.4\,ms^{-1}$ $137\,K$ (case 4) jet of nitrogen issuing into a chamber at $298\,K$ and $3.97\,MPa$. These laboratory flows have been modelled with LES. The real-gas models described above have been implemented into the computational fluid dynamics (CFD) code OpenFOAM. In contrast with previous density-based LES of supercritical flows [19–23], a pressure-based solution method is employed. The pressure-based real-gas implementation by Jarczyk [15] is accurate and highly efficient for low Mach number flows such as the experiment studied by Mayer [5]. The viscous heating term $\partial\tau_{ij}u_i/\partial x_j$ is negligible for low velocity flows and it has not been included in the modelling. Verification and validation of the numerical model is presented in [15].

3.3.1. *SGS models*

The LES neglects sub-grid fluctuations during the evaluation of the filtered thermodynamic and transport properties. Eddy-viscosity modelling has been used for the sub-grid fluxes. The effective viscosity and conductivity are then composed of a laminar and a turbulent part: $\mu_{\text{eff}} = \mu(\bar{\phi}) + \mu_{\text{SGS}}$ and $\lambda_{\text{eff}} = \lambda(\bar{\phi}) + \lambda_{\text{SGS}}$ respectively. The sub-grid

scale (SGS) viscosity and thermal conductivity are modeled for the results shown below using a Smagorinsky model. Here μ_{SGS} is determined by

$$\mu_{SGS} = (C_S\Delta)^2\sqrt{\bar{S}_{ij}\bar{S}_{ij}} \tag{3.8}$$

$\bar{S}_{ij}$ is the strain-rate tensor of the filtered quantities, Δ is the mesh size and C_S is the Smagorinsky constant, which has been set to a value of 0.17. The sub-grid scale thermal conductivity is then calculated using the turbulent Prandtl number Pr_t which has been given a value of 1.0 here,

$$\lambda_{SGS} = \frac{\mu_{SGS}c_p}{Pr_t}. \tag{3.9}$$

3.3.2. *Computational set up*

The experimental mixing chamber is a square duct of $60 \times 60mm$ with a length of about one meter. The injector has a diameter of $2.2mm$ and a length that assures a fully turbulent pipe flow at the injector exit. The numerical setup for the jet investigations is the same used by Schmitt *et al.* [24]. The injector diameter is identical to the experiment and the chamber was given a length of $250mm$. For the investigations shown below, the mixing chamber has been assumed to be rotationally symmetric and it was given a diameter of $122mm$. The geometry has been discretized using an O-grid with a total number of cells of about 1.7 million. The grid has been refined near the injector region, where the cell size is between $0.1mm$ and $0.15mm$.

At the inlet a time varying fully turbulent velocity profile extracted from a turbulent pipe flow has been prescribed. The chamber front wall has been assumed to be adiabatic and the outer chamber walls were given a constant temperature of $298K$. A wave transmissive boundary condition has been prescribed at the outlet. Further details of the numerical set-up are provided in Ref. [15].

4. Results and discussion

4.1. *Analysis of thermal inhomogeneity*

The effects of transcritical real gas properties have been investigated first in the case of a constant pressure system with an inhomogeneous temperature distribution. This simple system is useful for analysing fluid property effects that may be relevant to LES modelling of the Mayer *et al.* case – drawing an analogy between the thermally inhomogeneous fluid studied here and a mass of fluid inside a LES filter volume. The fluid system is defined by a fixed pressure (3.97 MPa) and by specifying a distribution of temperature. For the purposes of this exploratory study a Gaussian mass distribution function of temperature has been assumed, where the fraction of mass in the system with temperature T is given by:

$$f(T) = \frac{1}{\sqrt{2\pi T''^2}}\exp\left[-\frac{(T-\bar{T})}{2T''^2}\right]. \tag{4.1}$$

$\bar{T}$ and T''^2 are the mean and variance of T.

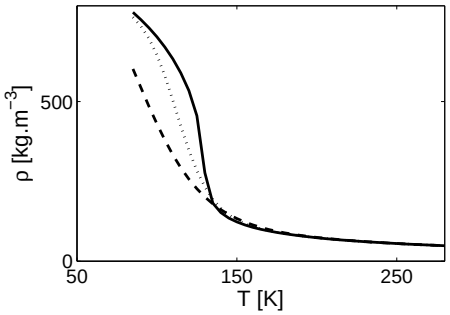

FIGURE 3. Mean density of a thermally inhomogeneous system at 3.97 MPa, with $T'' = 0$K (–), $15K$ (.), and $30K$ (- -).

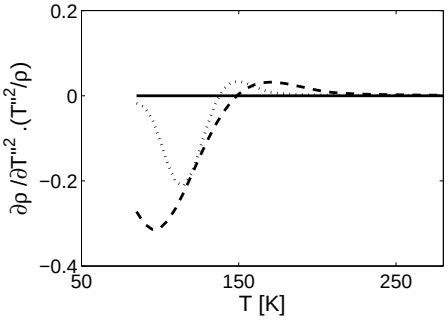

FIGURE 4. Fractional change in density due to a fractional change in the temperature variance, legend as in Fig. 3.

4.1.1. *Density and dilatation*

Favre mean values of a property X can be computed by integrating over the mass distribution function:

$$\bar{X} = \int_0^\infty f(T) X . dT. \tag{4.2}$$

Since $f(T)$ is a mass density function, the mean density should be evaluated by first using Eq. (4.2) to find the specific volume (i.e. $X = 1/\rho$), and then computing the mean density as $\bar{\rho} = 1/\bar{X}$. The mean density is plotted in Fig. 3 as a function of the mean temperature for $T'' = 0, 15,$ and $30\,K$.

Due to the non-linear relationship between temperature and specific volume the mean density in Fig. 3 depends on both the mean and variance of the temperature. Note that the ideal gas equation of state implies a linear relationship between specific volume and temperature (at constant pressure), so that the mean density of an ideal gas does not depend on the temperature variance. Above the pseudo-boiling temperature ($130\,K$ at $3.97\,MPa$ in Fig. 3) real gas effects diminish and the density dependence on temperature variance can be neglected. The implication of the dependence on temperature variance for LES modelling is that sub-grid temperature (or density) variation should be considered when computing the mean density (or temperature).

A further implication of the dependence of the density on temperature variance is that thermal dissipation within the LES filter volume tends to reduce the sub-grid temperature variance, providing a source term for the filtered density. Differentiating the mean density with respect to temperature variance, and non-dimensionalising with $T''^2/\hat{\rho}$ provides a measure of the fractional density change occurring during one dissipation time-scale. The non-dimensionalised fractional density change is plotted in Fig. 4; the fractional density change can be order-unity in the vicinity of the pseudo-boiling temperature, depending on the temperature variance. The fractional density change is mostly negative (mixing reduces the variance and tends to increase the mean density), and its magnitude decreases to zero as the temperature variance decays to zero.

Thermal dissipation causes both positive and negative dilatation of the flow, and the impact of this dilatation on the fluid dynamcis and modelling of transcritical flow needs to be assessed. By analogy with the dilatation produced in thin premixed flame fronts, we speculate that the dilatation in transcritical high density gradient magnitude (HDGM) layers may be expected to provide a significant hydrodynamic contribution to the sub-

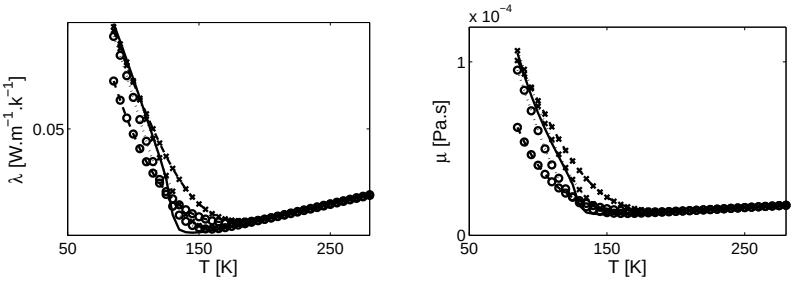

FIGURE 5. Mean thermal conductivity and dynamic viscosity for a thermally inhomogeneous system at 3.97 MPa, with $T'' = 0$K (–), $15K$ (.), and $30K$ (- -). Favre averages: (x); $\mu_{\mathrm{eff},\perp}$ and λ_{eff}: (o).

grid scalar flux (both gradient or counter gradient in nature depending on the correlation between the scalar and the dilatation fluctuations for the fluid system in question [26]). Noting that, in the absence of surface tension, an evaporating liquid-gas interface is unconditionally unstable to Darrieus–Landau-type hydrodynamic instabilities [27] the dilatation of transcritical fluid may also lead to instability of the HDGM layers, if not limited by the stabilising process of density gradient dissipation. It is not clear whether either this hydrodynamic flux or this hydrodynamic instability can be neglected for all supercritical fluid systems *a priori* and further analysis is required.

4.1.2. *Transport properties*

The influence of temperature inhomogeneities on the averaged transport properties have also been analysed in the inhomogeneous constant pressure system. Filtered transport properties are needed in LES to compute the resolved contribution of molecular transport. The mass-weighted *Favre* mean thermal conductivity or dynamic viscosity is found from Eq. (4.2) with $X = \lambda$ or $X = \mu$, respectively. The thermal conductivity and the dynamic viscosity both exhibit non-linear relationships with temperature so, as seen for density, the Favre mean thermal conductivity and dynamic viscosity depend on the temperature variance, as seen in Fig. 5. The influence of temperature fluctuations on the Favre mean transport properties becomes significant at low temperatures close to the pseudo-boiling temperature. While it is usually safe to neglect the effect of sub-grid temperature fluctuations on transport properties in LES of sub-critical fluids, neglect of temperature fluctuations in transcritical fluid can lead to greater than 100% error in the Favre averaged properties.

In LES of transcritical fluid, however, even using the Favre filtered transport coefficients may lead to errors in computation of molecular transport: consider a contrived flow configuration illustrated in Fig. 6 in which there is a one-dimensional variation of temperature along the vertical direction within a LES filter volume. There is a corresponding one-dimensional and non-linear variation of the transport properties as a function of temperature (and at constant pressure). The resolved velocity field strains this fluid both parallel and normal to the temperature gradient, and heat transfer occurs in the direction of the resolved temperature gradient.

An effective molecular viscosity can be defined based on the resolved shear strain and stress components:

$$\mu_{\mathrm{mol,ij}} = \frac{\tau_{ij} L_j}{\Delta u_i}, \tag{4.3}$$

and an effective thermal conductivity can be defined based on the resolved temperature

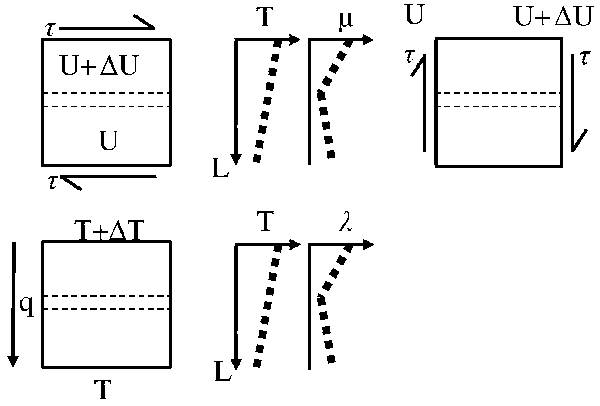

FIGURE 6. Illustration of transport property variation in fluid with a one-dimensional temperature stratification. Top left: fluid with shear stress perpendicular to the temperature gradient; top centre, temperature and viscosity variation; top right, fluid with shear stress parallel to the temperature gradient; bottom left, fluid with heat flux q; bottom centre, temperature and conductivity variation.

gradient and the grid-scale heat flux:

$$\lambda_{\mathrm{mol,j}} = \frac{\bar{q}_j L_j}{\Delta T}. \tag{4.4}$$

L_j is the length of the filter volume in the j direction.

In the situation where the shear stresses and heat fluxes are uniform throughout the volume, the effective molecular viscosity for shear stresses normal to the temperature gradient is:

$$\frac{1}{\mu_{\mathrm{mol},\perp}} = \int_0^\infty f(T)\frac{1}{\mu(T)}.dT. \tag{4.5}$$

The effective molecular viscosity for shear stresses parallel to the temperature gradient equals the Favre average viscosity:

$$\mu_{\mathrm{mol},\parallel} = \int_0^\infty f(T)\mu(T).dT. \tag{4.6}$$

Therefore, if the temperature field in a transcritical fluid is stratified (at least at the scale of an LES grid cell), the effective viscosity is anisotropic. Note that the viscosity is at its minimum close to the pseudo-boiling temperature (the dotted region in Fig. 6) meaning that the fluid can slip preferentially along the pseudo-boiling surface and thereby reduce the effective viscosity for shear perpendicular to the temperature gradient. The Favre average gives the correct effective viscosity for shear parallel to the temperature gradient, but for all other orientations between the temperature and the shear the Favre average overestimates the effective viscosity. Since shear stresses in stratified turbulent flow tend to align normal to high density gradients [25], $\mu_{\mathrm{eff},\perp}$ may provide a better model for the effective viscosity in turbulent flows than the Favre average, and further investigation of the effective viscosity in turbulent flows is needed.

Since heat transfer occurs along the direction of the resolved temperature gradient, the effective conductivity is:

$$\frac{1}{\lambda_{\mathrm{mol}}} = \int_0^\infty f(T)\frac{1}{\lambda(T)}.dT. \tag{4.7}$$

This model for the effective conductivity differs from the Favre average conductivity; the low thermal conductivity in the vicinity of the pseudo-boiling temperature provides a layer of thermal insulation, reducing the rate of heat transfer below that predicted by the Favre average conductivity $\tilde{\lambda}$.

Values of $\mu_{\mathrm{mol},\perp}$, $\mu_{\mathrm{mol},\parallel} = \tilde{\mu}$, $\tilde{\lambda}$, and λ_{mol} are plotted as a function of mean and rms temperature in Fig. 5 for the constant pressure inhomogeneous system. Close to the pseudo-boiling temperature, both the conductivity and the viscosity deviate significantly from the zero-variance values, as well as depending on the orientation of the temperature gradient. Since grid-scale molecular transport is often significant in LES, it is necessary to investigate the modelling of the effective transport properties further in turbulent transcritical flow.

4.2. *Analysis of a transcritical counterflow*

The transcritical counterflow configuration has been analysed to quantify the errors associated with different methods for computing the filtered density. Mixture fraction as defined in Sec. 3.2 is shown in Fig. 7 for the reference case. A box filter has been applied with filter size $\Delta = 5\delta_\rho = 2.0 \times 10^{-5} m$, where δ_ρ is the thickness of the mixing layer based on the maximum density gradient; the filtered mixture fraction ($\tilde{Z}$) and the segregation ($\tilde{Z}(1-\tilde{Z})$) are also shown in Fig. 7. The filter size has been chosen so that the mixing layer is partially resolved.

4.2.1. *Density closure*

Using the $5\delta_\rho$ box filter, the filtered density has been evaluated and modelled in three ways (Fig. 8): Eqs. (2.12), (2.14), and (2.15). The first model (Eq. (2.12)) neglects sub-filter fluctuations of thermodynamic properties. Second, the flamelet approach (Eq. (2.15)) is applied, where a presumed β-function distribution of mixture fraction is tested, taking the filtered mean and variance of mixture fraction from the counterflow solution. Third, the first-order model by Taskinoglu *et al.* [4] (Eq. (2.14)) is compared. Even though the mixing layer is partially resolved, the error due to neglecting sub-grid fluctuations and also the error due to the first-order model exceed 20% in the vicinity of the pseudo-boiling temperature (Z=0.1). The flamelet model appears to perform adequately in this unchallenging test; because the density is a function of the mixture fraction, the inaccuracy of the flamelet model is due entirely to differences between β-function presumed mixture fraction distribution and the sub-filter distribution of mixture fraction in the counterflow. Among the three models considered, the flamelet model appears to have most potential for achieving good accuracy in flows that can be characterised by two-stream mixing. The accuracy of the flamelet approach depends on the availability of suitable models for the probability density function of mixture fraction. The usual β-function modelling of the mixture fraction PDF remains to be validated for turbulent flow at transcritical conditions.

4.3. *Transcritical fluid injection*

4.3.1. *Main flow features*

The transcritical nitrogen jet configuration investigated experimentally by Mayer *et al.* [5] has been simulated as described above. A Schlieren visualisation of the predicted flow field for case 3 in Fig. 9 indicates the presence of well defined HDGM regions in the near-field of the jet. The centreline density predictions for the transcritical case 3, and the supercritical case 4, are compared with experimental measurements in Fig. 10. The

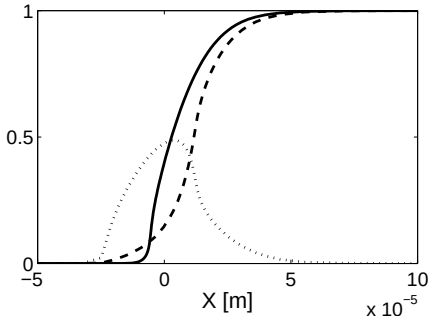

FIGURE 7. Mixture fraction Z (–), filtered mixture fraction $\hat{Z}$ (- -), and mixture fraction segregation $\hat{Z}(1-\hat{Z})$ (..) in the base counterflow case. $\Delta = 5\delta_\rho$.

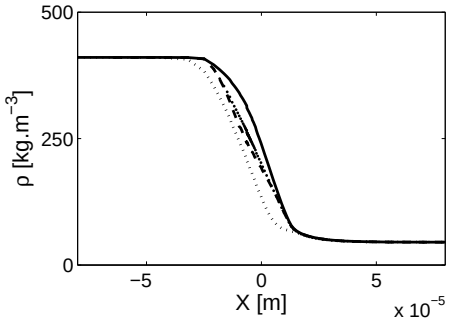

FIGURE 8. The filtered density $\hat{\rho}$ (•) in the base counterflow case, and models: $\rho(\hat{h})$ (–), Flamelet (- -), 1$^{\text{st}}$ Order (..).

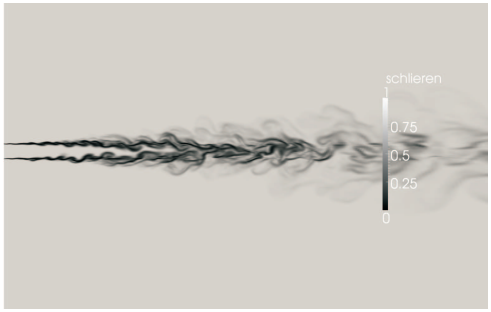

FIGURE 9. Numerically generated instantaneous Schlieren image based on the resolved density gradient from the LES of case 3.

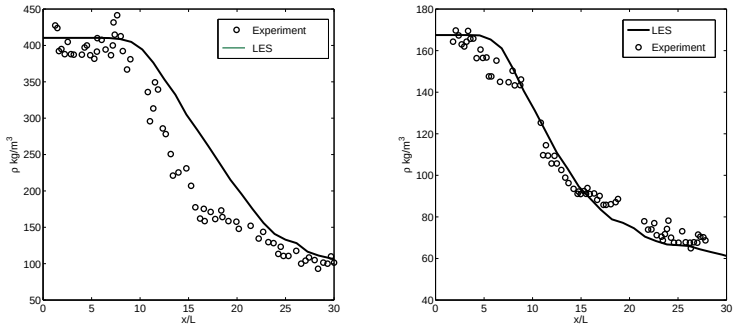

FIGURE 10. Measured and simulated centreline density variation for the Mayer *et al.* turbulent nitrogen jet case 3 (left) and 4 (right).

agreement is excellent for the supercritical case 4 but the increase in jet penetration for the high-density transcritical case is over predicted marginally. This highlights the difficulties associated with modelling the physics associated with the large property gradients occurring in transcritical flows. Detailed discussion of the flow physics predicted is provided in Ref. [15].

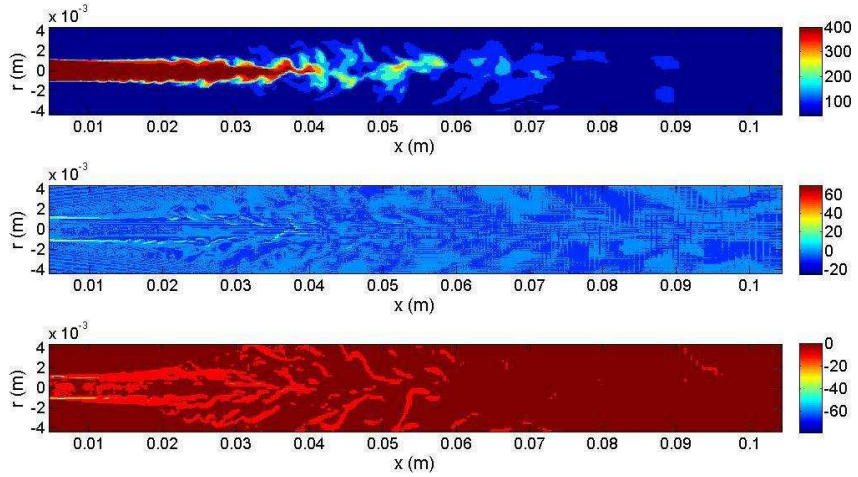

FIGURE 11. Instantaneous density contours neglecting sub-grid fluctuations (top), first-order correction (middle), presumed-PDF correction (bottom) (kg/m^3) Mayer *et al.* case 3 [5].

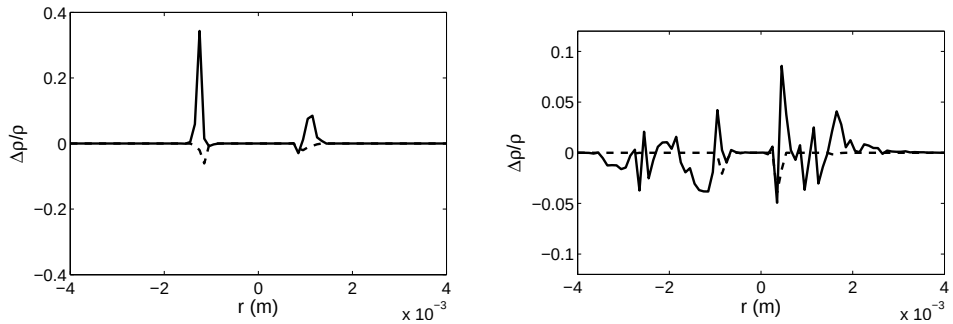

FIGURE 12. Radial profiles of the normalised instantaneous density corrections (Flamelet (- -), 1st order (–)) at axial position x=0.01m (left) and x=0.022m(right).

4.3.2. *Evaluation of the density closure*

The three approaches discussed in Sec. 2.2.2 for evaluating the filtered density from the other resolved variables have been compared in Mayer *et al.* 's case 3. The three density closures (Eqs. (2.12), (2.14), and (2.15)) are computed by post processing an instantaneous solution field from the LES (which itself employs Eq. (2.12)). This comparison does not show the effects of the density closure on the flow field, rather it gives an indication of the order of magnitude of the corrections to the density that arise due to use of the first-order (Eq. (2.14)) and the presumed-PDF (Eq. (2.15)) closures. The first-order correction involves an explicit filtering of the resolved LES fields, which has been performed using the OpenFOAM 'Simple' filtering operation, which corresponds to a box filter of two times the LES grid size. The enthalpy variance needed to generate the presumed-PDF has been estimated using a constant value scale-similarity model (Eq. (2.24) in Ref. [4]). Contour plots of the simulated density field, and the corrections due to the first-order and presumed-PDF closures are shown in Fig. 11.

Radial profiles of the density corrections are also shown in Fig. 12 at two axial positions in the near-field of the jet.

Both the first-order and the presumed-PDF approaches provide a leading-order correction to the filtered density (and consequently to its derivatives) in the HDGM regions. The corrections provided by the two methods however are not in agreement. The first-order model produces a less smooth correction, perhaps because the LES filter size is greater than the eight DNS grid-scales for which the first-order correction has been validated previously [4]. The presumed-PDF approach however is expected to work robustly irrespective of filter size. A full *a posteriori* evaluation of the respective models will be required in order to make any conclusions about the relative validity of any of the three approaches.

5. Conclusions

The effects of real-gas properties on transcritical thermal mixing of nitrogen have been analysed in the context of Large Eddy Simulation. The simulations used for this analysis employ a volume-corrected Peng-Robinson real-gas equation of state, and real-gas transport models.

It has been demonstrated that, because of the non-linear relationship between temperature and specific volume at low temperatures in the vicinity of the pseudo-boiling temperature, the mean or filtered density of a real gas depends strongly on sub-filter temperature variations. Further, we have introduced a metric, $\partial\bar{\rho}/\partial T''^2.(T''^2/\bar{\rho})$, which measures the impact of thermal dissipation on the filtered density value. The metric indicates that, in the vicinity of the critical temperature, thermal dissipation leads to an important source term for filtered density. Dissipation processes in turbulent transcritical flows have not been thoroughly investigated however, and this finding motivates further investigation.

Sub-filter temperature stratification causes anisotropy in the effective molecular viscosity – reducing the effective viscosity for shear normal to the temperature gradient, and similarly reducing the effective thermal conductivity below its mean value. Since it is expected that shear is usually strongest normal to steep density gradients, the proposed expression for the effective molecular viscosity perpendicular to the temperature gradient appears to be an appropriate model for the effect of temperature stratification on the effective viscosity. An model for the effective thermal conductivity is also provided, and both of these models should now be tested.

Two models for the effects of sub-grid fluctuations on the filtered density have been analysed in a laminar counterflow and a turbulent jet configuration. The analysis in the counterflow suggests that the flamelet modelling approach is more robust given large filter sizes, while the analysis of the turbulent jet shows that the correction term is of leading order. The importance of sub-grid fluctuations to the values of filtered transport and thermodynamic properties motivates further development of the presumed-PDF modelling approach.

Acknowledgments

Financial support has been provided by the German Research Foundation (Deutsche Forschungsgemeinschaft – DFG) in the framework of the Sonderforschungsbereich Transregio 40 and the IGSSE (International Graduate School of Science and Engineering) at Technische Universität München. Computational resources have generously been provided by the Leibniz-Rechenzentrum München (LRZ). E. S. Richardson re-

ceived support during this work from the UK Engineering and Physical Sciences Research Council [grant number EP/I004564/1].

References

[1] SELLE, L. C., OKONG'O, N. A., BELLAN, J. AND HARSTAD, K. G. (2007). Modelling of sub-grid scale phenomena in supercritical transitional mixing layers: an a priori study. *J. Fluid Mech.*, **596**, 57–91.

[2] SELLE, L. AND RIBERT, G. (2008). Modeling requirements for large-eddy simulation of turbulent flows under supercritical thermodynamic conditions. In: *Proc. CTR Summer Program 2008*, 195–207.

[3] SELLE, L. AND SCHMITT, T. (2010). Large-Eddy Simulation of Single-Species Flows under Supercritical Thermodynamic Conditions. *Combust. Sci. Tech.*, **182**(4), 392–404.

[4] TASKINOGLU, E. S. AND BELLAN, J. (2010). A posteriori study using a DNS database describing fluid disintegration and binary-species mixing under supercritical pressure: heptane and nitrogen. *J. Fluid Mech.*, **645**, 211-254.

[5] MAYER W., TELLAR J., BRANAM R., SCHNEIDER G. AND HUSSONG J. (2003). Raman measurement of cryogenic injection at supercritical pressure. *J. Heat and Mass Trans.*, **37**, 709–719.

[6] LEMMON, E. W., MCLINDEN, M. O. AND FRIEND, D. G. (2011). Thermophysical Properties of Fluid Systems. In: Linstrom, P. J. and Mallard, W. G. (Eds.), *NIST Chemistry WebBook, NIST Standard Reference Database Number 69.*, National Institute of Standards and Technology, Gaithersburg MD, 20899, http://webbook.nist.gov.

[7] RIBERT, G., JARCZYK, M., NIEDERMEIER, C. A., PETIT, X., PFITZNER, M., SCHMID, M. AND SATTELMAYER, T. (2011). Supercritical Fluid Flow Injection. *SFB/TRR40 – Proc. Summer Program 2011*, 15–26.

[8] SMAGORINSKY, J. (1963). General circulation experiments with the primitive equations. Part 1. basic experiments. *Mon. Weather Rev.*, **91**, 99–164.

[9] CLARK, R., FERZIGER, J. AND REYNOLDS, W. (1979). Evaluation of sub-grid-scale models using an accurately simulated turbulent flow. *J. Fluid Mech.*, **91**(1), 1–16.

[10] BARDINA, J., FERZIGER, J. AND REYNOLDS, W. (1980). Improved sub-grid scale models for large eddy simulation. *AIAA*, **80**, 1357.

[11] PETERS, N. (2000). *Turbulent Combustion*. Cambridge University Press.

[12] CUTRONE, L., DE PALMA, P., PASCAZIO, G. AND NAPOLITANO, M. (2010). A RANS flamelet-progress-variable method for computing reacting flows of real-gas mixtures. *Computers and Fluids*, **39**, 485–498.

[13] POHL, S., JARCZYK, M. AND PFITZNER, M. (2011). A real gas laminar flamelet combustion model for the CFD-Simulation of LOX/GH2 combustion. *Proc. European Combustion Meeting*, July 28–31, Cardiff, UK.

[14] COSILAB, V. 3.1. (2010). *Rotexo Software.*, Bochum.

[15] JARCZYK, M. AND PFITZNER, M. (2011). Large eddy simulation of supercritical nitrogen jets. Submitted to *AIAA*.

[16] PENG, D.-Y. AND ROBINSON, P. D. (1976). A New Two-Constant Equation of State. *Industrial Engineering and Chemical Fundamentals*, **15**(1), 59–64.

[17] HARSTAD, K. G., MILLER, R. S. AND BELLAN, J. (1997). Efficient high-pressure state equations. *AIChE J.*, **43**(6), 1605–1610.

[18] CHUNG, T.-H., AJLAN, M., LEE, L. L. AND STARLING, K. E. (1988). Generalized multiparameter correlation for nonpolar and polar fluid transport properties. *Ind. Eng. Chem. Res.*, **27**(4), 671–679.

[19] SCHMITT, T., RUIZ, A., SELLE, L. AND CUENOT, B. (2010). Large-Eddy Simulation of Supercritical-Pressure Round Jets. *AIAA J.*, **48**(9), 2133–2144.

[20] SCHMITT T., RUIZ, A., SELLE, L. AND CANDEL, S. (2011). Large-Eddy Simulation of Oxygen/Methane Flames Under Transcritical Conditions. *Proc. Combust. Inst*, **33**, 1383–1390.

[21] ZONG, N. AND YANG, V. (2006). Cryogenic Fluid Jets and Mixing Layers in Transcritical and Supercritical Environments. *Comb. Sci. Tech.*, **178**, 193–227.

[22] OEFELEIN, J. (2006). Mixing and Combustion of Cryogenic Oxygen-Hydrogen Shear-Coaxial Jet Flames at Supercritical Pressure. *Comb. Sci. Tech.*, **178**, 229–252.

[23] MATSUYAMA, S., SHINJO, J., OGAWA, S. AND MIZOBUCHI, Y. (2010). Large Eddy Simulation of LOX/GH2 Shear-Coaxial Jet Flame at Supercritical Pressure. *AIAA 2010–208*.

[24] SCHMITT, T., RUIZ, A., SELLE, L. AND CUENOT, B. (2009). Large-Eddy Simulation of Transcritical Round Jets. *3rd EUCASS Conference* .

[25] HANNOUN, I. A., FERNANDO, H. J. S. AND LIST, E. J. (1988). Turbulence structure near a sharp density interface. *J. Fluid Mech.*, **189**, 189–209.

[26] SWAMINATHAN, N., BILGER, R. W. AND CUENOT, B. (2005). Relationship between turbulent scalar flux and conditional dilatation in premixed flames with complex chemistry. *Combust. Flame*, **126**, 1764–1779.

[27] ZENG, P., PITSCH, H., BINNINGER, B., PETERS, N. AND HERRMANN, M. (2011). Numerical Investigation of the Primary Atomization of Turbulent Liquid Jet with Evaporation under Diesel Engine Conditions. *24th Annual Conference on Liquid Atomization and Spray Systems*, Estoril, Portugal.